Dynamics of Majorana tetron qubits under quasiparticle poisoning

Sauri Bhattacharyya and Bernard van Heck
Dipartimento di Fisica, Sapienza Università di Roma, Piazzale Aldo Moro 2, 00185 Rome, Italy

(Received 30 August 2026; revised 31 October 2026; accepted 5 November 2026; published 18 November 2026)

We study the dissipative dynamics of a Majorana tetron qubit in the presence of extrinsic quasiparticle poisoning due to the coupling to external leads. From the Bloch-Redfield equation describing a finite-size topological superconductor hosting four Majorana zero modes and tunnel-coupled to fermionic reservoirs, we recover analytical expressions for the decoherence rate of a Majorana qubit at arbitrary values of the charging energy. The analysis shows that the exponential suppression of the decoherence rate is gradually removed by the energy splitting of the qubit states. These results can be useful to understand time-domain experimental data in Majorana qubit prototypes.

DOI: 10.1103/1d2y-fpbl

I. INTRODUCTION

In fault-tolerant quantum computation based on Majorana zero modes [1,2], qubits are encoded in the joint fermion parity of well-separated Majorana zero modes in a gapped topological superconductor [3]. The separation between Majorana zero modes ensures that the computational states are degenerate in energy, up to corrections $\propto e^{-L/\xi}$ at Majorana distances $L \gg \xi$, the coherence length in the topological phase. Even then, fermionic excitations may lead to computational errors due to *quasiparticle poisoning*. However, in thermal equilibrium the energy gap Δ makes the likelihood of their presence exponentially small, $\propto e^{-\Delta/T}$ with $T \ll \Delta$.

Taken together, these two conditions provide the topological protection [4,5] that underpins the prediction of long coherence times [6]. In real devices, it remains necessary to eliminate other forms of quasiparticle poisoning which do not originate from thermally excited quasiparticles in the superconductor. These may originate from external fermionic reservoirs (sometimes referred to as *extrinsic* quasiparticle poisoning [7–9]), as well as from the out-of-equilibrium population of above-gap excitations (*intrinsic* quasiparticle poisoning [10,11]).

To mitigate extrinsic quasiparticle poisoning, scalable proposals based on semiconductor-superconductor heterostructures [12–14] rely on the charging energy of a mesoscopic superconducting island [15], which assigns a finite energy cost to the addition or removal of a charge e to the island. If we call this energy cost U, the quasiparticle poisoning rates should be suppressed by an exponential factor $\propto e^{-U/T}$, restoring the topological protection provided that $T \ll U$.

The scalable logical unit of such proposals is the *tetron*, a superconducting island hosting four Majorana zero modes [13] (see also Refs. [16–18]). In a tetron, one bit of quantum information can be encoded in the two degenerate ground states of the island, and all required quantum operations can be executed via projective fermion parity measurements on different pairs of Majorana zero modes.

Early prototypes of tetron devices have been realized experimentally in InAs–Al [19,20] and InAs-Pb heterostructures [21]. While the tuning of these devices into a genuine topological phase is made difficult by disorder and remains strongly debated [22–24], on the more technical side both continuous parity monitoring as well as single-shot parity measurements via dispersive readout mediated by a quantum dot have been reported [20,25]. Time-domain fermion parity measurements have also been reported [26,27] on minimal Kitaev chains realized with hybrid quantum dot arrays [28–30], which can be used to realize tetronlike devices [31,32].

These developments will hopefully lead to the experimental study of quantum dynamics and decoherence in Majorana-based qubits, whose characterization will precede their use in quantum information processing. It is therefore a good time to study such devices from an open quantum system perspective [33].

In this work, we provide a quantitative theory of the dynamics of a Majorana tetron qubit subject to extrinsic quasiparticle poisoning. Although it is well known that all sources of extrinsic quasiparticle poisoning must be minimized in Majorana-based devices, this may not always be possible, especially in current devices that need transport contacts for the tuning of the topological phase. Our theory provides an explicit derivation of the exponential protection from decoherence of a Majorana qubit as well as, crucially, the departure from topological protection away from the ideal-case scenario.

II. THE MODEL

As depicted in Fig. 1, a tetron device consists of a topological superconducting island hosting four Majorana zero modes. We imagine that the four Majorana zero modes are

Published by the American Physical Society under the terms of the Creative Commons Attribution 4.0 International license. Further distribution of this work must maintain attribution to the author(s) and the published article's title, journal citation, and DOI.

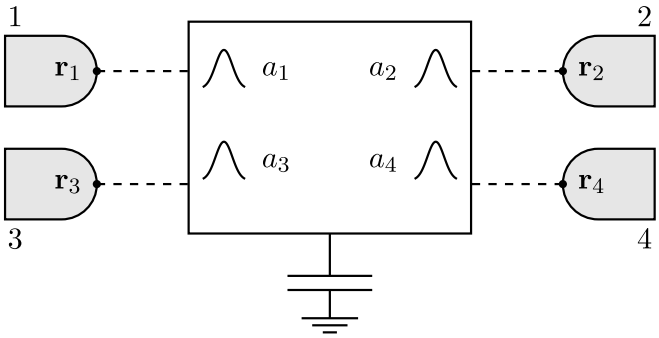


FIG. 1. A schematic diagram of a tetron device: A floating superconducting island (white box) contains four localized Majorana zero modes a_1, a_2, a_3, a_4. The superconductor is tunnel-coupled (dashed lines) to four fermionic leads (gray).

coupled to fermionic leads which act as an external source of quasiparticles. In experimental setups, they may serve the purpose of transport probes for the topological superconductor, or be part of the measurement apparatus for fermion parity measurements on the tetron.

The four well-separated Majorana zero modes are represented by Hermitian operators a_i obeying

$$\{a_i, a_j\} = \delta_{ij}, \tag{1}$$

for $i, j = 1, \ldots, 4$. Because these modes are the local degrees of freedom nonlocally encoding a qubit, we shall refer to them as the computational Majorana modes.

A. Hamiltonian

We adopt the following effective Hamiltonian to describe the quantum dynamics of the computational Majorana zero modes:

$$H = H_A + H_{AB} + H_B. \tag{2}$$

The first term describes the tetron in isolation from the leads:

$$H_A = \frac{i}{2}\sum_{ij} A_{ij} a_i a_j + 2U a_1 a_2 a_3 a_4. \tag{3}$$

The quadratic part of H_A contains the direct couplings among the computational Majoranas, gathered in the 4×4 matrix A, which by construction is real and antisymmetric ($A_{ij} = -A_{ji}$). The direct couplings are nonzero due to the finite spatial extent of the zero modes and the finite size of the tetron. The interaction term, which has a strength U, ensues from the finite capacitance to ground of the superconducting island hosting the Majoranas. It is proportional to the total fermion parity of the Majorana zero modes,

$$P = -4a_1 a_2 a_3 a_4, \tag{4}$$

which is equal to $P = +1$ for even-parity states and $P = -1$ for odd-parity states. This form of the charging interaction derives from the usual expression $\propto (N - n_g)^2$ of the charging energy of a floating superconducting island, restricted to the two-lowest energy charge states, one for each parity sector. This restriction assumes that other charge states as well as other quasiparticle states within the island are energetically inaccessible. This requires the quasiparticle energy gap to be much higher than temperature. Further conditions regarding the regime of validity of our calculations are stated in Sec. II B.

The computational Majorana zero modes are coupled to four fermionic leads by single particle tunneling. For simplicity we adopt a point contact model, in which each of the four reservoirs contacts the tetron at a single position $\mathbf{r}_i$. This is described by the second term H_{AB}:

$$H_{AB} = \sum_{ij} w_{ij}\, a_i\, c(\mathbf{r}_j) + \text{H.c.}, \tag{5}$$

where w_{ij} is a complex tunneling amplitude and $c(\mathbf{r}_j)$ annihilates a fermion in the j-th reservoir at position $\mathbf{r}_j$ (see Fig. 1). It is useful to write the tunneling Hamiltonian in the form $H_{AB} = -i\sum_i a_i B_i$, with Hermitian channel operators

$$B_i = i\sum_j w_{ij} c(\mathbf{r}_j) - w_{ij}^* c^\dagger(\mathbf{r}_j). \tag{6}$$

Note that this Hamiltonian allows a single Majorana zero mode to couple to multiple leads. We will often, however, invoke a simplifying assumption that a_i couples only to lead i, and that the coupling strengths are all equal. This corresponds to the choice

$$w_{ij} = w\,\delta_{ij} \tag{7}$$

for some complex amplitude w, so that the channel operator is reduced to the simpler form $B_i = w\, c(\mathbf{r}_i) - w^*\, c^\dagger(\mathbf{r}_i)$. In Sec. V C, we consider a scenario in which this assumption is relaxed.

The third term H_B is the Hamiltonian of the leads, which are assumed to be gapless and in thermal equilibrium at a temperature T. Rather than the specific form of H_B, it is useful to present the correlation function relevant for the open system dynamics, which is

$$C_{ij}(t) = \frac{1}{Z}\,\mathrm{Tr}_B[B_i(t) B_j(0) e^{-\beta H_B}] \tag{8}$$

with $B_i(t) = e^{iH_B t} B_i e^{-iH_B t}$, $Z = \mathrm{Tr}_B e^{-\beta H_B}$, and $\beta = 1/T$. By the cyclicity of the trace, the equilibrium correlation function obeys the Kubo-Martin-Schwinger condition

$$C_{ij}(t) = C_{ji}(-t - i\beta), \tag{9}$$

as well as $C_{ji}(t) = C_{ij}^*(-t)$. If the couplings take the simple form of Eq. (7), and if the leads are themselves assumed to be all identical, the correlation function factorizes as

$$C_{ij}(t) = \delta_{ij}\, C(t), \tag{10}$$

and we only have a single function $C(t)$ to characterize. The bath correlation function is studied in more detail in Appendixes B and C.

B. Time and energy scales

In general, the behavior of $C(t)$ is controlled by two time scales: one pertaining to the bath and one to the system-bath coupling strength w. The first is the bath correlation time τ_B, formally defined as [34,35]

$$\tau_B = \frac{\int_0^\infty t|C(t)|dt}{\int_0^\infty |C(t)|dt}. \tag{11}$$

For a wide-band fermionic reservoir in thermal equilibrium, as shown in Appendix C, the bath correlation time scale is controlled by temperature:

$$\tau_B^{-1} \approx \pi T. \tag{12}$$

Importantly, τ_B is independent from the system-bath coupling strength w. The latter determines instead a bare timescale for the bath-induced decoherence of the system, which we indicate as τ_D:

$$\tau_D^{-1} = \int_0^\infty |C(t)| dt. \tag{13}$$

Again in Appendix C, we show that this time scale is controlled by the tunneling rate between the system and the reservoir:

$$\tau_D^{-1} \approx \Gamma_0, \quad \Gamma_0 = 2\pi |w|^2 \nu(0), \tag{14}$$

with $\nu(0)$ the density of states in the leads at the Fermi level.

In Sec. IV we derive the master equation for the system under the assumption of weak system-bath coupling, which allows us to employ the Born-Markov approximation, valid under the condition

$$\tau_D \gg \tau_B. \tag{15}$$

For our fermionic reservoirs, this is equivalent to

$$\Gamma_0 \ll T. \tag{16}$$

Two additional energy scales determine the dynamics of the tetron in isolation, which is discussed in detail in Sec. III: the interaction U and the magnitude of the overlap couplings A_{ij}, which we can characterize by the energy scale

$$\epsilon = \max |A_{ij}|. \tag{17}$$

The regime of topological protection of the Majorana qubit corresponds to the following hierarchy of time scales,

$$\epsilon \ll \Gamma_0 \ll T \ll U. \tag{18}$$

We refer to this regime as the *degenerate* regime. It is studied in Sec. V, which covers the open system dynamics under the assumption $\epsilon \ll \Gamma_0$.

The regime of topological protection is gradually removed upon increasing ϵ. In Sec. VI we study the master equation in the regime $\epsilon \gg \Gamma_0$, which we refer to as the *secular* regime. We then show that the validity of the results can be extended across intermediate values $\epsilon \sim \Gamma_0$, all the way to the degenerate limit. The results of both Secs. V and VI apply to arbitrary ratios U/T, always provided that $T \gg \Gamma_0$.

III. UNITARY DYNAMICS OF THE TETRON

Before analyzing the open dynamics of the tetron, it is useful to examine the unitary dynamics under the isolated system Hamiltonian H_A. The spectrum of H_A is obtained by using an orthogonal matrix O to put the matrix A into canonical form,

$$OAO^T = \begin{bmatrix} 0 & \epsilon_1 & 0 & 0 \\ -\epsilon_1 & 0 & 0 & 0 \\ 0 & 0 & 0 & \epsilon_2 \\ 0 & 0 & -\epsilon_2 & 0 \end{bmatrix}. \tag{19}$$

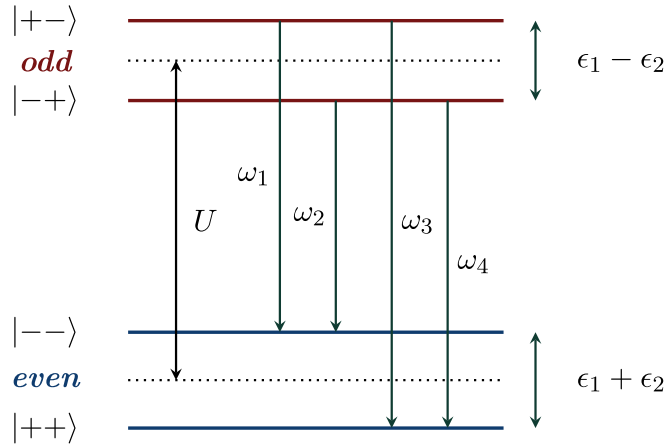


FIG. 2. The energy-level scheme of the isolated Majorana system. It comprises of a low-energy even-parity doublet, and a high-energy odd-parity one. The intradoublet splittings are due to the direct couplings among the zero modes, while the interdoublet gap is due to interactions. The dotted lines show the transitions corresponding to the four positive Bohr frequencies of Eqs. (28).

Without loss of generality, we assume $\epsilon_1 > \epsilon_2 > 0$. In terms of the operators $\tilde{a} = Oa$, one has

$$H_A = i\epsilon_1 \tilde{a}_1 \tilde{a}_2 + i\epsilon_2 \tilde{a}_3 \tilde{a}_4 + 2U \tilde{a}_1 \tilde{a}_2 \tilde{a}_3 \tilde{a}_4. \tag{20}$$

The three operators in H_A commute with each other and so the spectrum is easily constructed. It is convenient to introduce joint parity operators in the eigenbasis,

$$\tilde{P}_{ij} = -2i\tilde{a}_i \tilde{a}_j, \tag{21}$$

which have eigenvalues ± 1, depending on whether a fermionic mode $(\tilde{a}_i + i\tilde{a}_j)/\sqrt{2}$ is empty or occupied. Note that $P = \tilde{P}_{12}\tilde{P}_{34}$, so that

$$H_A = -\tfrac{1}{2}\epsilon_1 \tilde{P}_{12} - \tfrac{1}{2}\epsilon_2 \tilde{P}_{34} - \tfrac{1}{2}U \tilde{P}_{12}\tilde{P}_{34}. \tag{22}$$

We can therefore label the eigenstates of H_A as $|\sigma\tau\rangle$ with $\sigma = \pm 1$ the eigenvalues of $\tilde{P}_{12}$ and $\tau = \pm 1$ the eigenvalue of $\tilde{P}_{34}$. Their energies are (see Fig. 2)

$$E_{\sigma\tau} = -\tfrac{1}{2}(\sigma\epsilon_1 + \tau\epsilon_2) - \tfrac{1}{2}U\sigma\tau \tag{23}$$

and their total parity is $P = \sigma\tau$. The even and odd sectors of the spectrum are separated by a gap U, which is the origin of the protection from quasiparticle poisoning. We assume that $U > 0$ so that the ground state has even parity.

The unitary time evolution of parity observables under H_A is easy to compute. Working in the Heisenberg picture, we obtain

$$\tilde{P}_{12}(t) = \tilde{P}_{12}(0), \tag{24a}$$

$$\tilde{P}_{13}(t) = \tilde{P}_{13}(0)\cos[(\epsilon_1 + \epsilon_2)t] + \tilde{P}_{23}(0)\sin[(\epsilon_1 + \epsilon_2)t], \tag{24b}$$

$$\tilde{P}_{14}(t) = \tilde{P}_{14}(0)\cos[(\epsilon_1 - \epsilon_2)t] + \tilde{P}_{24}(0)\sin[(\epsilon_1 - \epsilon_2)t]. \tag{24c}$$

The time evolution of the remaining parity operators under H_A follows from the conservation of the total parity P. Indeed, the

conservation of P gives the operator identities

$$\tilde{P}_{34} = P\tilde{P}_{12}, \quad \tilde{P}_{24} = -P\tilde{P}_{13}, \quad \tilde{P}_{23} = P\tilde{P}_{14}. \tag{25}$$

The physical interpretation of Eqs. (24) and (25) is the following: $\tilde{P}_{12}$ and $\tilde{P}_{34}$ are constant-in-time populations of the fermionic modes $c_1 = (\tilde{a}_1 + i\tilde{a}_2)/\sqrt{2}$ and $c_2 = (\tilde{a}_3 + i\tilde{a}_4)/\sqrt{2}$, whereas the other parity operators are precessing coherences between eigenstates of the same total parity.

In discussing dynamics, we may be interested in the time evolution of joint parity operators of *computational* Majorana zero modes,

$$P_{ij} = -2ia_i a_j, \tag{26}$$

rather than in that of the eigenmodes. Indeed, ideally it is the P_{ij} which are the observables accessible by parity measurement in a tetron device. Using the orthogonal transformation O, one obtains

$$P_{ij}(t) = \sum_{ij} O^T_{ii'} O^T_{jj'} \tilde{P}_{i'j'}(t). \tag{27}$$

From this list of basic results, we may collect the following useful observations about the unitary dynamics of parity observables in the tetron. First, the energy gap U does not enter the time evolution of $P_{ij}(t)$. Second, joint parities of computational Majorana zero modes in general undergo precession at a frequency that depends on the total parity P. Third, in terms of computational Majorana zero modes it is not always possible to make a distinction between populations and coherences. This is only possible if the degeneracy is broken and the eigenmodes coincide with the computational ones.

A qubit may be encoded in the two even-parity eigenstates, $|++\rangle$ and $|--\rangle$. In the topologically protected regime, as already mentioned, ϵ_1 and ϵ_2 are exponentially small. In the ideal limit in which they vanish, the qubit states are degenerate, there is no precession dynamics and no distinction between the computational modes and the eigenmodes. Furthermore, the conservation of total parity in the closed system prevents qubit leakage to the odd-parity sector formed by $|+-\rangle$ and $|-+\rangle$.

Upon introducing the coupling to the external leads, the total parity of the system is no longer conserved, as the tunneling terms in H_{AB} can change it. This introduces a leakage timescale out of the qubit subspace. The coupling to the external leads will also be a source of decoherence within the qubit subspace, that must be added to any dephasing that may occur due to noise in ϵ_1, ϵ_2 [36]. To determine the timescales associated with leakage and decoherence, we must move on to the study of the open quantum system dynamics.

IV. BLOCH-REDFIELD EQUATION

Single-particle tunneling between the superconducting island forming the tetron and the reservoirs causes the total parity to change. There are four possible transitions from an initial state of odd parity to a final state of even parity. They have the following Bohr transition frequencies (see Fig. 2):

$$|+-\rangle \to |--\rangle : \quad \omega_1 = E_{+-} - E_{--} = U - \epsilon_1, \tag{28a}$$
$$|-+\rangle \to |--\rangle : \quad \omega_2 = E_{-+} - E_{--} = U - \epsilon_2, \tag{28b}$$
$$|+-\rangle \to |++\rangle : \quad \omega_3 = E_{+-} - E_{++} = U + \epsilon_2, \tag{28c}$$
$$|-+\rangle \to |++\rangle : \quad \omega_4 = E_{-+} - E_{++} = U + \epsilon_1. \tag{28d}$$

Note that the transition frequencies ω_s are defined as the energy of the initial state minus that of the final state. Reversed transitions—from an even parity state to an odd parity state—have opposite transition frequency. With this convention, a positive transition frequency corresponds to the release of energy from the tetron into the bath, and thus as an absorption process from the point of view of the reservoir. On the other hand, a negative transition frequency corresponds to the emission of energy from the bath into the tetron.

The odd-to-even transition frequencies ω_s are all positive if $U > \epsilon_1 > \epsilon_2$, which is the case depicted in Fig. 2. If U becomes smaller than ϵ_1, then the energy spectrum does not separate anymore into two parity-doublets, but it alternates between even and odd energy levels. In this case, ω_1 becomes negative. If U is smaller than both ϵ_1 and ϵ_2, then the odd doublet is sandwiched between the two even levels, and both ω_1 and ω_2 are negative.

In general, each of these transitions may be activated by tunneling into or out of any of the computational Majorana zero modes. Such a process may be described by a jump operator

$$A_{i,s} = \Pi_{\sigma'_s\tau'_s} a_i \Pi_{\sigma_s\tau_s}, \quad (s = 1, 2, 3, 4), \tag{29}$$

where $\Pi_{\sigma\tau}$ is a projector onto the eigenstate $|\sigma\tau\rangle$,

$$\Pi_{\sigma\tau} = |\sigma\tau\rangle\langle\sigma\tau| = \tfrac{1}{4}(1 + \sigma\tilde{P}_{12})(1 + \tau\tilde{P}_{34}), \tag{30}$$

and $\{\sigma_s, \tau_s\}$, $\{\sigma'_s, \tau'_s\}$ are the quantum numbers of the initial and final states involved in the transition s. In total, there are 16 jump operators A_i, each of them a linear combination of terms with one or three a_i's.

Using these jump operators, it is possible to formulate a local-in-time master equation for the evolution of the density matrix of the computational Majorana zero modes, $\rho(t)$. In doing so, we assume that the initial reduced density matrix $\rho(0)$ commutes with the total parity P,

$$[\rho(0), P] = 0, \tag{31}$$

so that it does not contain coherences between the even-parity and odd-parity sectors: $\langle\sigma\tau|\rho(0)|\sigma'\tau'\rangle = 0$ if $|\sigma\tau\rangle$ and $|\sigma'\tau'\rangle$ are states of opposite parity. Because, as already discussed, the coherent evolution preserves the total parity, once true at $t = 0$ this property remains true at all subsequent times: $[\rho(t), P] = 0$. We can therefore always decompose the density matrix into an even and an odd part: $\rho = \rho_e + \rho_o$, with

$$\rho_e = \tfrac{1}{2}(1 + P)\rho \quad \text{and} \quad \rho_o = \tfrac{1}{2}(1 - P), \tag{32}$$

which will sometimes come in handy. Note that Eq. (31) does not prevent population transfer from the even to the odd sector or vice versa, which can and indeed does happen.

Working in the weak coupling limit where $\tau_D \gg \tau_B$, a local-in-time master equation can be derived by invoking the Born-Markov approximation, within a standard open quantum

systems approach [33]. The detailed derivation is presented in Appendix C and yields the following Bloch-Redfield master equation for $\rho(t)$ in the interaction picture:

$$\frac{d\rho}{dt} = -\frac{1}{4}\sum_{i,j}\sum_{s,s'}[e^{i\delta_{ss'}t}\,\Gamma_{ij}(\omega_s)(A^\dagger_{i,s'}A_{j,s}\rho - A_{j,s}\,\rho\,A^\dagger_{i,s'}) + e^{-i\delta_{ss'}t}\,\Gamma_{ji}(-\omega_s)(A_{i,s'}A^\dagger_{j,s}\rho - A^\dagger_{j,s}\,\rho\,A_{i,s'}) + \text{H.c.}], \tag{33}$$

with $\delta_{ss'} = \omega_{s'} - \omega_s$ and

$$\Gamma_{ij}(\omega) = \int_0^\infty dt\,\exp(i\omega t)C_{ij}(t) \tag{34}$$

the one-sided Fourier transform of the correlation function. As customary [33], we split it into its Hermitian and anti-Hermitian parts,

$$\Gamma_{ij}(\omega) = \tfrac{1}{2}\gamma_{ij}(\omega) + iS_{ij}(\omega) \tag{35}$$

with

$$\gamma_{ij}(\omega) = \Gamma_{ij}(\omega) + \Gamma^*_{ji}(\omega), \tag{36}$$

$$S_{ij}(\omega) = [\Gamma_{ij}(\omega) - \Gamma^*_{ji}(\omega)]/2i. \tag{37}$$

The anti-Hermitian part of the correlation function, $S_{ij}(\omega)$, gives rise to the Lamb shift corrections to the unitary dynamics of the system. The Lamb shift terms arising from $S_{ij}(\omega)$ commute by construction with the system Hamiltonian H_A: Their effect is only to shift the energy levels ϵ_1 and ϵ_2, and the corresponding precession frequencies in Eqs. (24). As we are interested in the dissipative effects induced by the reservoirs, we neglect the Lamb shift terms from now own.

We therefore focus on the Hermitian part $\gamma_{ij}(\omega)$, which is the Fourier transform of $C_{ij}(t)$,

$$\gamma_{ij}(\omega) = \int_{-\infty}^\infty e^{i\omega t}C_{ij}(t)\,dt. \tag{38}$$

In virtue of the Kubo-Martin-Schwinger condition (9), it satisfies detailed balance, namely

$$\gamma_{ji}(-\omega) = e^{-\beta\omega}\gamma_{ij}(\omega). \tag{39}$$

Furthermore, at fixed frequency ω, the matrix $\gamma_{ij}(\omega)$ is positive.

If one makes the simplifying assumption that $w_{ij} = w\,\delta_{ij}$ [Eq. (7)], then $\gamma_{ij}(\omega) = \gamma(\omega)\delta_{ij}$. In Appendix B, we show that

$$\gamma(\omega) = 2\pi|w|^2\,\frac{\nu(\omega)+\nu(-\omega)}{1+e^{-\beta\omega}}, \tag{40}$$

where $\nu(\epsilon)$ is the density of states in the leads. If one can approximate $\nu(\omega)\approx\nu(0)$, which is likely to be a good approximation for a wide-band lead given that the transition frequencies are all of order U, then

$$\gamma(\omega) = \frac{2\Gamma_0}{1+e^{-\beta\omega}}, \tag{41}$$

with the tunneling rate Γ_0 defined in Eq. (14). We will often invoke this simple version of $\gamma(\omega)$ to obtain concrete formulas.

The Bloch-Redfield equation (33) is not in the Gorini-Kossakowski-Sudarshan-Lindblad (GKSL) form and thus it is not guaranteed to preserve the positivity of the density matrix. This is due to the presence of the oscillatory factors $\exp(i\delta_{ss'}t)$, which couple transitions associated with different Bohr frequencies. In our model, the frequency differences take the following possible values:

$$\delta_{11} = \delta_{22} = \delta_{33} = \delta_{44} = 0, \tag{42a}$$

$$\delta_{12} = \delta_{34} = -\delta_{21} = -\delta_{43} = \epsilon_1 - \epsilon_2, \tag{42b}$$

$$\delta_{13} = \delta_{24} = -\delta_{31} = -\delta_{42} = \epsilon_1 + \epsilon_2, \tag{42c}$$

$$\delta_{14} = -\delta_{41} = 2\epsilon_1, \tag{42d}$$

$$\delta_{23} = -\delta_{32} = 2\epsilon_2. \tag{42e}$$

We note that the frequency differences *do not* contain U, which is the scale of the gap between the two parity sectors. This is owing to the fact that the allowed processes flip the total parity successively in opposite directions.

Making further progress on the solution of the Bloch-Redfield equation requires some assumption on $\delta_{ss'}$, and thus essentially ϵ, compared to the other energy scales. Referring to the nomenclature introduced in Sec. II, we distinguish between the *degenerate regime* in which all the phase factors can be well approximated with unity over the entire time evolution, and a *secular regime* in which the phase factors average out unless $\delta_{ss'} = 0$. The degenerate regime holds when the direct couplings between Majorana zero modes are very small, $\epsilon \ll \Gamma_0$, and so it includes with the regime of topological protection. The secular regime, instead, becomes relevant when $\epsilon \gg \Gamma_0$.

V. THE DEGENERATE REGIME

A. The ideal case: Perfect degeneracy

In the ideal scenario behind the design of the tetron, the computational Majorana zero modes are so well separated that all the couplings A_{ij} in the Hamiltonian H_A can be set to zero, so that $H_A = -(U/2)\,P$. Then, the spectrum consists of doubly degenerate even and odd energy levels ($\epsilon_1 = \epsilon_2 = 0$), separated by an energy gap U. With this spectral information as input, and in the simple case in which $\Gamma_{ij}(\omega) = \delta_{ij}\Gamma(\omega)$ [Eq. (7)], the Bloch-Redfield equation (33) simplifies to

$$\frac{d}{dt}\rho = -\frac{1}{4}\sum_{i,s,s'}[\Gamma(U)(A^\dagger_{i,s'}A_{i,s}\rho - A_{i,s}\,\rho\,A^\dagger_{i,s'}) + \Gamma(-U)(A_{i,s'}A^\dagger_{i,s}\rho - A^\dagger_{i,s}\,\rho\,A_{i,s'}) + \text{H.c.}]. \tag{43}$$

With all transition frequencies degenerate, the sums over s and s' can be performed noting that

$$\sum_s A_{is} = \frac{1}{2}\,a_i\,(1-P). \tag{44}$$

After the substitution $\Gamma(U) = \frac{1}{2}\gamma(U) + iS(U)$ and a bit of algebra (which, in fact, causes all terms proportional to $S(U)$ to drop out), one arrives at

$$\frac{d\rho}{dt} = \mathcal{D}_0[\rho] \tag{45}$$

with a dissipator in the GKSL form,

$$\mathcal{D}_0[\rho] = -\frac{\gamma(U)}{2}\left[\rho_o - \frac{1}{2}\sum_i a_i\,\rho_o\,a_i\right] - \frac{\gamma(-U)}{2}\left[\rho_e - \frac{1}{2}\sum_i a_i\,\rho_e\,a_i\right]. \tag{46}$$

Due to the degeneracy of energy levels in the even and odd sectors there is no preferred basis in which to solve the master equation. Nevertheless, to make contact with the calculations in following sections, it is convenient to work in the basis $|\sigma\tau\rangle$ of common eigenstates of P_{12} and P_{34}, with $\sigma = \pm$ now the eigenvalue of P_{12} and $\tau = \pm$ the eigenvalue of P_{34}.

An important feature of the dynamics is that the diagonal and off-diagonal elements of the reduced density matrix evolve separately. Following usual nomenclature, we refer to the diagonal matrix elements as *populations* and to the off-diagonal as *coherences*, although we emphasize that in the presence of degeneracy the distinction between the two is a matter of convention (a basis choice).

Because of the superselection rule (31), there are only two nontrivial coherences in the density matrix, one per parity sector:

$$c_e = \langle{+}{+}|\rho|{-}{-}\rangle, \tag{47a}$$

$$c_o = \langle{-}{+}|\rho|{+}{-}\rangle. \tag{47b}$$

In the even parity sector, we find

$$\frac{dc_e}{dt} = -\Gamma_e\,c_e \tag{48}$$

with

$$\Gamma_e = \frac{\gamma(-U)}{2} = \Gamma_0\,(1+e^{\beta U})^{-1}. \tag{49}$$

In the last equality, we have invoked Eq. (41). In the odd parity sector, instead, we find

$$\frac{dc_o}{dt} = -\Gamma_o\,c_o \tag{50}$$

with

$$\Gamma_o = \frac{\gamma(U)}{2} = \Gamma_0\,(1+e^{-\beta U})^{-1}. \tag{51}$$

We recover the crucial result: In the protected regime $\beta U \gg 1$, $\Gamma_e \approx \Gamma_0 e^{-\beta U}$ is exponentially suppressed compared to Γ_0. On the other hand, Γ_o always remains $\approx\Gamma_0$. The key factors behind this result are the presence of an energy gap in the spectrum and the detailed balance obeyed by the bath correlation function in thermal equilibrium.

The populations, defined as

$$p_{\sigma\tau} = \mathrm{Tr}(\Pi_{\sigma\tau}\rho) = \langle\sigma\tau|\rho|\sigma\tau\rangle, \tag{52}$$

satisfy the following system of rate equations:

$$\frac{d}{dt}\begin{bmatrix} p_{-+} \\ p_{+-} \\ p_{++} \\ p_{--} \end{bmatrix} = \frac{1}{2}\begin{bmatrix} -2\Gamma_o & 0 & \Gamma_e & \Gamma_e \\ 0 & -2\Gamma_o & \Gamma_e & \Gamma_e \\ \Gamma_o & \Gamma_o & -2\Gamma_e & 0 \\ \Gamma_o & \Gamma_o & 0 & -2\Gamma_e \end{bmatrix}\begin{bmatrix} p_{-+} \\ p_{+-} \\ p_{++} \\ p_{--} \end{bmatrix}. \tag{53}$$

The steady state—the unique zero mode of the rate equations—is a thermal average of the even and odd sectors,

$$\rho_\infty = \frac{(\Pi_{--}+\Pi_{++}) + e^{-\beta U}(\Pi_{-+}+\Pi_{+-})}{2+2e^{-\beta U}}. \tag{54}$$

The approach to the steady state is controlled by the nonzero eigenvalues of the rate equation matrix, which are Γ_o, Γ_e and $\Gamma_o + \Gamma_e = \Gamma_0$.

Rather than presenting an explicit solution for $\rho(t)$, it more instructive to compute directly the time evolution of parity observables, which can be gathered from the above results. The expected value of the total parity P obeys

$$\frac{d}{dt}\langle P\rangle = \Gamma_o(1-\langle P\rangle) - \Gamma_e(1+\langle P\rangle). \tag{55}$$

The solution is

$$\langle P(t)\rangle = e^{-\Gamma_0 t}\langle P(0)\rangle + (1-e^{-\Gamma_0 t})P_\infty \tag{56}$$

with

$$P_\infty = \frac{1-e^{-\beta U}}{1+e^{-\beta U}}. \tag{57}$$

We see that in the protected regime $\beta U \gg 1$ the total amount of leakage out of the qubit subspace is suppressed exponentially: $1 - P_\infty \approx e^{-\beta U}$. This exponentially small amount of leakage occurs at a rate Γ_0.

The time evolution of the expectation values of the parity operators $P_{ij} = -2ia_ia_j$ is conditioned on the initial total parity P:

$$\langle P_{ij}(t)\rangle = \begin{cases} \langle P_{ij}(0)\rangle\, e^{-\Gamma_e t} & \text{if} \quad P(0) = +1, \\ \langle P_{ij}(0)\rangle\, e^{-\Gamma_o t} & \text{if} \quad P(0) = -1. \end{cases} \tag{58}$$

These relations hold for all values of i and j: Since the qubit is encoded in two degenerate states, there is no distinction between relaxation and dephasing, and the decoherence of all qubit operators is set by the protected timescale Γ_e.

B. Near degeneracy

How do these results change in the presence of small couplings A_{ij}, which split the parity degeneracy of the energy spectrum? We argue that there is a regime of weak overlaps, roughly speaking $\epsilon \ll \Gamma_0$, where results do not change qualitatively from the ideal case just presented.

First, if the energies ϵ_1 and ϵ_2 resulting from the tunneling between Majorana zero modes are small compared to U, then it is possible to approximate

$$\Gamma(U \pm \epsilon_1) \approx \Gamma(U \pm \epsilon_2) \approx \Gamma(U) \tag{59}$$

and similarly for $\Gamma(-U)$. In other words, the energy splittings do not affect considerably the transition strengths entering the dissipator of the Bloch-Redfield equation.

Second, the transition frequency differences $\delta_{ss'}$ listed in Eq. (42) are all of the order of ϵ_1 or ϵ_2: nonzero but small in the scenario under consideration. Thus, the resulting oscillations in the dissipator of the Bloch-Redfield are slow. The corresponding phase factors can be put to one, provided that $|\delta_{ss'}\tau_D| \ll 1$, which means $|\epsilon_1 \pm \epsilon_2| \ll \Gamma_0$.

Under these conditions, the dissipator of the Bloch-Redfield equation remains the same as in the ideal case of Eq. (43). Unlike the ideal case, however, the unitary dynamics of the tetron is not trivial, and coherent precession of the parity operators occurs with frequencies $\omega_\pm = \epsilon_1 \pm \epsilon_2$, as discussed in Sec. III.

We note that since $\Gamma_e \ll \Gamma_0$ if $\beta U \gg 1$, the above-mentioned conditions are compatible with the condition $\Gamma_e \lesssim \epsilon$. Thus, because the even parity sector decoheres very slowly, coherent oscillations may still be measurable in the time domain even when ϵ_1 and ϵ_2 may not be resolved in, e.g., tunneling spectroscopy.

C. The zero-energy extended state scenario

We now consider a situation in which the Majorana zero modes a_1 and a_2 form an extended Andreev bound state at zero energy which can couple to two leads, while a_3 and a_4 remain well localized and coupled only to lead 3 and 4 respectively. This scenario is interesting because extended Andreev bound states very close to zero energy can be tricky to distinguish from well-separated Majorana zero modes, as discussed, for instance, in Ref. [37]. Other than this modification to the system-bath couplings, we keep neglecting all direct couplings among the Majorana modes, and so we remain in the degenerate regime.

In Appendix B we show that, under some simplifying assumptions, this scenario can be modeled via the correlation function

$$\gamma_{ij}(\omega) = \gamma(\omega)\,(\delta_{ij} + \lambda\,\delta_{i1}\delta_{j2} + \lambda\,\delta_{i2}\delta_{j1}). \tag{60}$$

Here, λ is a dimensionless parameter taking values in the interval $[-1, 1]$. It controls the relative strength of the tunneling rates between a_1 and a_2 and the leads. When $\lambda = 0$, a_1 is coupled only to lead 1, while when $|\lambda| = 1$, a_1 is coupled equally strongly to leads 1 and 2. The same applies to the tunneling rates between a_2 and the leads. We note that this parametrization preserves the positivity condition of $\gamma_{ij}(\omega)$.

The simplifying assumptions behind this form of the system-bath couplings are the following. First, as in the previous calculations in this section, we have assumed identical tunneling rates between a_i and lead i. Second, we have assumed that the density of states in the leads is particle-hole symmetric, $\nu(\epsilon) = \nu(-\epsilon)$. This, in particular, allows λ to be real.

The presence of an extended state gives rise to a nonzero value of λ and thus to a finite cross correlation $\gamma_{12}(\omega)$. The master equation in the degenerate regime must be supplemented by a new term;

$$\frac{d\rho}{dt} = \mathcal{D}_0[\rho] + \lambda\,\mathcal{D}_1[\rho] \tag{61}$$

with

$$\mathcal{D}_1[\rho] = \frac{\gamma(U)}{4}\,[a_2\rho_o\,a_1 + a_1\rho_o\,a_2] + \frac{\gamma(-U)}{4}\,[a_2\rho_e\,a_1 + a_1\rho_e\,a_2]. \tag{62}$$

The addition of $\mathcal{D}_1[\rho]$ does not modify the rate equations for the populations, Eq. (53). However, it affects the time evolution of the coherences c_e and c_o defined in Eq. (47). Namely, Eqs. (48) and (50) must be supplemented with the following *coupled* system of equations

$$\frac{d}{dt}\begin{bmatrix} c_o \\ c_e \end{bmatrix} = \frac{1}{2}\begin{bmatrix} -2\Gamma_o & i\lambda\Gamma_e \\ -i\lambda\Gamma_o & -2\Gamma_e \end{bmatrix}\begin{bmatrix} c_o \\ c_e \end{bmatrix}. \tag{63}$$

We see that a finite λ induces a transfer of coherence between the two parity sectors. Indeed, c_o and c_e do not evolve separately under the decay rates Γ_o and Γ_e, but jointly under the new decay rates (eigenvalues of the 2×2 matrix above)

$$\Gamma_\pm = \tfrac{1}{2}\Gamma_0\,(1 \pm \kappa) \tag{64}$$

with

$$\kappa^2 = \left(\frac{\Gamma_o - \Gamma_e}{\Gamma_0}\right)^2 + \lambda^2\,\frac{\Gamma_e\Gamma_o}{\Gamma_0^2}. \tag{65}$$

Let us imagine that we initialize the system in the even parity sector, so that $c_o(0) = 0$. Then, the time evolution of the coherences is

$$c_o(t) = -ic_e(0)\,\frac{\lambda}{\kappa}\,\frac{\Gamma_e}{\Gamma_0}\,\exp\left(-\frac{1}{2}\Gamma_0 t\right)\,\sinh\left(\frac{1}{2}\kappa\Gamma_0 t\right), \tag{66}$$

$$c_e(t) = c_e(0)\left[\left(\frac{\kappa\Gamma_0 + \Gamma_e - \Gamma_o}{2\kappa\Gamma_0}\right)\exp\left(-\Gamma_+ t\right) + \left(\frac{\kappa\Gamma_0 - \Gamma_e + \Gamma_o}{2\kappa\Gamma_0}\right)\exp\left(-\Gamma_- t\right)\right]. \tag{67}$$

We see that a finite λ turns the simple exponential decay of the coherence in Sec. V A into a biexponential decay, because it couples two decoherence channels which were previously independent.

Note that, at finite λ, one has $\Gamma_+ > \Gamma_o$ and $\Gamma_- < \Gamma_e$. In other words, increasing $|\lambda|$ from zero, Γ_+ tends to increase from Γ_o, while Γ_- decreases from Γ_e, reaching $\Gamma_- = \frac{1}{2}\Gamma_e$ at $\lambda = 1$. Due to the decrease in Γ_-, we can say that the cross-correlation slows down the decoherence. In fact, in a scenario where a_3 and a_4 are also extended zero modes, one can tune the rate Γ_- to be arbitrarily close to zero [38].

How do these results on populations and coherences translate into the evolution of parity observables? Because the rate equations for the populations are independent of λ, the time dependence of the total parity P and the "longitudinal" parities P_{12} and P_{34} is unaffected with respect to the results of Sec. V A. On the other hand, the "transverse" parity observables $P_{13}, P_{14}, P_{23}, P_{24}$ inherit the biexponential decay of the coherences.

VI. THE SECULAR REGIME

We now analyze the case in which the energies ϵ_1 and ϵ_2 become larger than the system-bath coupling strength:

$$\epsilon \gg \Gamma_0. \tag{68}$$

In this regime, the Bohr transition frequencies of the tetron can be resolved by the bath. It is then appropriate to invoke the conventional *secular approximation*, in which one neglects all terms in the Bloch-Redfield equation except those with $\delta_{ss'} = 0$. The idea is that for all terms with nonzero $\delta_{ss'}$, the inequality

$$|\delta_{ss'}\tau_D| \sim \epsilon\,\Gamma_0^{-1} \gg 1 \tag{69}$$

holds, and so the corresponding term averages out to zero over an evolution time of order τ_D.

To be concrete and keep the calculations transparent and analytically tractable, in this section we consider a simpler version of the system Hamiltonian H_A:

$$H_A = i\epsilon(a_1a_2 + a_3a_4) + 2U a_1a_2a_3a_4. \tag{70}$$

In this version, the computational Majorana zero modes coincide with the eigenmodes, and furthermore we have $\epsilon_1 = \epsilon_2 = \epsilon$. This choice introduces a finite energy splitting in the even-parity qubit subspace, the essential feature that we would like to capture in our results. On the other hand, the odd-parity subspace remains doubly degenerate, which eliminates unessential complications in the calculations. This scenario also captures a situation—relevant for current experimental designs—in which the tetron is realized from two distinct topological nanowire segments, the first hosting zero modes a_1 and a_2 and the second hosting a_3 and a_4, with interwire overlaps all but negligible.

For this simple version of the system Hamiltonian, the computational Majorana zero modes a_i coincide with the eigenmodes $\tilde{a}_i$, and the transition frequency differences split in two groups: Half of them are equal to 2ϵ, while the rest is equal to zero. The Bloch-Redfield equation can then be simplified considerably: with some algebra and patience—displayed in Appendix D—invoking the secular approximation then leads to the master equation:

$$\frac{d\rho}{dt} = \mathcal{D}_{\text{sec}}[\rho]. \tag{71}$$

The dissipator $\mathcal{D}_{\text{sec}}$, for disconnected and identical reservoirs such that $\gamma_{ij}(\omega) = \delta_{ij}\gamma(\omega)$, is

$$\begin{aligned}
&\mathcal{D}_{\text{sec}}[\rho] \\
&= -\frac{1}{4}\gamma(U-\epsilon)\left[\rho_{\text{o}} - \sum_i \Pi_{--}\, a_i\, \rho\, a_i\, \Pi_{--}\right] \\
&\quad - \frac{1}{4}\gamma(\epsilon-U)\left[\{\Pi_{--}, \rho\} - \sum_i a_i\, \Pi_{--}\, \rho\, \Pi_{--}\, a_i\right] \\
&\quad - \frac{1}{4}\gamma(U+\epsilon)\left[\rho_{\text{o}} - \sum_i \Pi_{++}\, a_i\, \rho\, a_i\, \Pi_{++}\right] \\
&\quad - \frac{1}{4}\gamma(-\epsilon-U)\left[\{\Pi_{++}, \rho\} - \sum_i a_i\, \Pi_{++}\, \rho\, \Pi_{++}\, a_i\right].
\end{aligned} \tag{72}$$

Unlike in the degenerate case discussed in the Sec. V, in this regime the distinction between population and coherences is physical: The common eigenstates of P_{12} and P_{34} provide a preferred basis as eigenstates of H_A. The advantage of having chosen this basis already to discuss the degenerate case is that the formulas below can be compared directly to the analogous one provided in Sec. V.

In fact, the coherences c_{e} and c_{o} obey the same evolution as before, see respectively Eq. (48) and Eq. (50), except that the decoherence rates Γ_{e} and Γ_{o} must be updated. In the even parity sector, we find

$$\Gamma_{\text{e}} = \tfrac{1}{4}[\gamma(\epsilon-U) + \gamma(-\epsilon-U)]. \tag{73}$$

Using Eq. (41), this expression reduces to

$$\Gamma_{\text{e}} = \frac{\Gamma_0}{2}\left[\frac{1}{1+e^{\beta(U-\epsilon)}} + \frac{1}{1+e^{\beta(U+\epsilon)}}\right]. \tag{74}$$

If $U > \epsilon$ and additionally $\beta(U-\epsilon) \gg 1$, the rate is well approximated by

$$\Gamma_{\text{e}} \approx \Gamma_0\, e^{-\beta U}\, \cosh(\beta\epsilon). \tag{75}$$

As we can see, in this regime the suppression of decoherence due to the interaction U is softened by the energy splitting ϵ. As ϵ increases, the topological protection is compromised. The exponential suppression of the decoherence rate disappears, even at low temperatures, once ϵ becomes comparable to or larger than U.

In the odd-parity sector, instead, we find

$$\Gamma_{\text{o}} = \tfrac{1}{4}[\gamma(U-\epsilon) + \gamma(U+\epsilon)]. \tag{76}$$

Using again Eq. (41), this expression becomes

$$\Gamma_{\text{o}} = \frac{\Gamma_0}{2}\left[\frac{1}{1+e^{-\beta(U-\epsilon)}} + \frac{1}{1+e^{-\beta(U+\epsilon)}}\right], \tag{77}$$

which is never exponentially smaller than Γ_0.

Conditioned on the initial total parity being even or odd, the decoherence rates Γ_{e} and Γ_{o} also control the time evolution of the "transverse" parity observables P_{13}, P_{14}, P_{23}, and P_{24}—those not associated with population of the energy levels.

The time evolution of the populations $p_{\sigma\tau}$ is more complex than in the degenerate case. Starting from the master equation (71), we find the following system of rate equations, which replaces Eq. (53):

$$\frac{d}{dt}\begin{bmatrix} p_{--} \\ p_{+-} \\ p_{-+} \\ p_{++} \end{bmatrix} = \frac{1}{4}\begin{bmatrix} -2\gamma(\epsilon-U) & \gamma(U-\epsilon) & \gamma(U-\epsilon) & 0 \\ \gamma(\epsilon-U) & -\gamma(U-\epsilon)-\gamma(U+\epsilon) & 0 & \gamma(-\epsilon-U) \\ \gamma(\epsilon-U) & 0 & -\gamma(U-\epsilon)-\gamma(U+\epsilon) & \gamma(-\epsilon-U) \\ 0 & \gamma(U+\epsilon) & \gamma(U+\epsilon) & -2\gamma(-\epsilon-U) \end{bmatrix}\begin{bmatrix} p_{--} \\ p_{+-} \\ p_{-+} \\ p_{++} \end{bmatrix}. \tag{78}$$

The steady state is now a Gibbs thermal state that takes into account the energy splitting ϵ,

$$\rho_\infty = \frac{e^{-\beta\epsilon}\Pi_{--} + e^{-\beta U}(\Pi_{-+} + \Pi_{+-}) + e^{\beta\epsilon}\Pi_{++}}{2\cosh(\beta\epsilon) + 2e^{-\beta U}}. \tag{79}$$

From the populations, we can obtain also the time evolution of the total parity P as well as the "longitudinal" parities P_{12} and P_{34}, since these parity observables are just linear combinations of projectors:

$$P = \Pi_{++} + \Pi_{--} - \Pi_{-+} - \Pi_{+-}, \tag{80a}$$

$$P_{12} = \Pi_{+-} + \Pi_{++} - \Pi_{--} - \Pi_{-+}, \tag{80b}$$

$$P_{34} = \Pi_{-+} + \Pi_{++} - \Pi_{--} - \Pi_{+-}. \tag{80c}$$

In particular, from Eq. (79) we can easily obtain their steady-state expectation values,

$$P_\infty = \frac{\cosh(\beta\epsilon) - e^{-\beta U}}{\cosh(\beta\epsilon) + e^{-\beta U}}, \tag{81}$$

and

$$P_{12}^\infty = P_{34}^\infty = \frac{\sinh(\beta\epsilon)}{\cosh(\beta\epsilon) + e^{-\beta U}}. \tag{82}$$

The approach to these steady state values is controlled by the nonzero eigenvalues of the matrix in Eq. (78). Using Eq. (41), these are given—analogously to the degenerate case—by Γ_o, Γ_e and their sum $\Gamma_o + \Gamma_e = \Gamma_0$.

The time evolution of the "longitudinal" coherences P_{12} and P_{34}, though quite convoluted to write for arbitrary initial states, becomes simple if we assume that the initial state is one of the two qubit states $|++\rangle$ or $|--\rangle$. Then, we have

$$\langle P_{12}(t)\rangle = \langle P_{34}(t)\rangle = \pm e^{-\Gamma_e t} + (1 - e^{-\Gamma_e t})P_{12}^\infty, \tag{83}$$

and so we see that the relaxation to the steady state occurs over the same timescale that dictates the dephasing of the qubit.

Relation to the universal Lindblad equation

It is quite immediate to notice that the dissipator in the secular regime, Eq. (72), is smoothly connected to that in the degenerate regime, Eq. (46), as one sends $\epsilon \to 0$. Naturally, this is also true of all the decoherence rates derived from the secular dissipator. One is therefore tempted to extend the regime validity of the formulas derived in the secular regime beyond the one in which they were originally derived, namely $\epsilon \gg \Gamma_0$.

For this purpose, we compared the secular master equation derived above with the universal Lindblad equation (ULE) [35]. The ULE is a positive and Markovian master equation: It is derived under the Born-Markov approximation $\tau_D \gg \tau_B$, but without making any type of approximation (such as the secular one $\epsilon \gg \Gamma_0$) which requires relating the spectral properties of the system with the strength of the system-bath coupling. In the context of Majorana zero modes, the ULE has been already applied to the study of tetron devices in Refs. [39,40].

For disconnected and identical reservoirs, $\gamma_{ij}(\omega) = \delta_{ij}\gamma(\omega)$, the ULE dissipator takes the form

$$\mathcal{D}_{\rm ULE}[\rho] = -\frac{1}{4}\sum_{i=1}^{4}\left(K_i\rho K_i^\dagger - \frac{1}{2}\{K_i^\dagger K_i, \rho\}\right), \tag{84}$$

with jump operators

$$K_i = \sum_{s=1}^{4}[\sqrt{\gamma(\omega_s)}A_{i,s} + \sqrt{\gamma(-\omega_s)}A_{i,s}^\dagger]. \tag{85}$$

In contrast to the secular master equation, a single ULE jump operator is composed of transitions at different Bohr frequencies and therefore generates interference terms between them in general. For the model considered in this section, Eq. (85) becomes

$$K_i = \sqrt{\gamma(U-\epsilon)}\,\Pi_{--}a_i + \sqrt{\gamma(\epsilon-U)}\,a_i\Pi_{--} + \sqrt{\gamma(U+\epsilon)}\,\Pi_{++}a_i + \sqrt{\gamma(-U-\epsilon)}\,a_i\Pi_{++}.. \tag{86}$$

As shown in Appendix E, all interference terms in $K_i^\dagger K_i$ vanish identically. In the recycling term $K_i\rho K_i^\dagger$, terms connecting different total-parity blocks vanish for density matrices satisfying $[\rho, P] = 0$. The remaining interference terms, which couple the two distinct Bohr frequencies $U-\epsilon$ and $U+\epsilon$, cancel after summing over the two Majoranas within each canonical pair. Consequently,

$$\mathcal{D}_{\rm ULE}[\rho] = \mathcal{D}_{\rm sec}[\rho]. \tag{87}$$

This equivalence shows that the regime of validity of the results obtained from the secular dissipator can be extended all the way to $\epsilon = 0$, and thus that they are smoothly connected with the results obtained in the degenerate regime, Sec. V.

VII. CONCLUSIONS

We have studied the dissipative dynamics of a Majorana tetron qubit under the presence of (extrinsic) quasiparticle poisoning, within the Born-Markov approximation. Our results are summarized by a formula for the decoherence rate of a Majorana qubit, Eq. (74):

$$\Gamma_e = \frac{\Gamma_0}{2}\left[\frac{1}{1+e^{\beta(U-\epsilon)}} + \frac{1}{1+e^{\beta(U+\epsilon)}}\right]. \tag{88}$$

The formula has a humble explanation: It is the absorption rate of a quasiparticle from the leads, averaged over the two even-parity qubit states. It illustrates the crossover outside of the topologically protected regime $\epsilon \ll \Gamma_0 \ll T \ll U$ as either the temperature or the energy splitting ϵ are increased. Considering the argument just made in Sec. VI A, its regime of validity is quite broad: The formula applies to arbitrary ratios ϵ/Γ_0, ϵ/U, and U/T, provided that $T \gg \Gamma_0$. The decoherence rate above applies to all qubit observables (i.e., bilinear parity operators) provided the tetron is initialized in an even parity state. In Secs. V and VI, we collected more analytical results on the rate equations, steady state and leakage rate governing the time evolution of the qubit.

If some of the Majorana zero modes have extended wave functions that couple to more than one lead, two or more relaxation channels become coupled and the decay of the decoherence transitions from a simple exponential to a multiexponential (see Sec. V C). This may help distinguish well-localized Majorana zero modes from zero-energy Andreev states which are extended throughout the entire device. It is amusing that a signature of the latter is a *slowdown* of decoherence due to quasiparticle poisoning. However, to this conclusion we have to add that an extended state is sensitive to other local sources of noise—not included in our analysis—to which well-separated Majorana zero modes are not.

We should also distinguish the zero-energy Andreev state treated in Sec. V C from the case of so-called quasi-Majorana

states [41]. In the latter case, a zero-energy Andreev state is formed by two Majorana zero modes which are coupled asymmetrically to the same lead. Because the couplings remain local in this case, the conclusions of Sec. V C are not applicable.

In our derivations, we have focused on a few scenarios that isolated qualitatively important factors—such as the finite energy splitting between qubit states and the presence of cross-correlations between leads. In doing so, we have allowed ourselves to make simplifying assumptions—such as taking individual tunneling rates for all the leads to be identical, or the energy splitting of odd-parity states to be zero—in order to arrive at simple analytical results that can guide understanding of the general case.

In full detail, the general case is probably amenable only to numerical analysis, which we leave for future work. Still, it can be argued that some simplifications can be relaxed with minor modifications from the results. For instance, introducing in Eq. (70) asymmetric couplings between a_1a_2 and a_3a_4 or small cross-couplings between – say – a_1a_3 and a_2a_4 would primarily introduce an energy splitting in the odd sector, as in the general case of Fig. 2. The main consequence would be that in Eq. (88) one would have an average over four terms with slightly different transition frequencies rather than just an average over two terms.

Our theory does not apply to *intrinsic* quasiparticle poisoning [10,11] related to the excitation of above-gap quasiparticles inside the topological superconducting island, nor to *extrinsic* quasiparticle poisoning due to a *nonequilibrium* population of quasiparticles in the external reservoirs. In fact, the detailed balance of Eq. (39) is the essential assumption which underpins the above derivation of exponentially protected decoherence rates.

The study of the open-system dynamics of tetron devices in the presence of a nonequilibrium distribution of quasiparticles represents an important theoretical problem to be tackled, for which the present work provides a baseline. Furthermore, to model realistic tetron devices it would be important to explicitly include the quantum dots used for the parity measurements, which may mediate the coupling between the tetsron and external leads [13]. Another interesting direction is the study of the error induced by quasiparticle poisoning on braiding operations, extending previous work based on parity-preserving noise sources [42–44].

ACKNOWLEDGMENTS

We thank Marco Grilli for nice and useful discussions on the project. S.B. acknowledges financial support from the PNRR MUR Project No. PE0000023-NQSTI, and specifically the project 'Topological Phases of Matter, Superconductivity, and Heterostructures' Partenariato Esteso 4-Spoke 5 (n. PE4221852A63A88D). We have used Gemini 3.6 Flash to generate the tikz source code for the figures in the main text, starting from our own hand-drawn sketches.

DATA AVAILABILITY

No data was generated or analyzed during this work.

APPENDIX A: DERIVATION OF THE BLOCH-REDFIELD EQUATION

The derivation of the Bloch-Redfield of Eq. (33) starting from the model Hamiltonian of Sec. II broadly follows the standard steps described, e.g., in Ref. [33]. We have already described it in detail for the case $U = 0$ in our previous work [38], and the first part of that derivation remains valid at finite U. Using the interaction picture with respect to $H_A + H_B$, truncating the von Neumann equation at second order in the system-bath coupling, taking the trace over the bath and employing the Born-Markov approximation, one arrives at

$$\dot{\rho} = -\frac{1}{4}\sum_{i,j=1}^{4}\left\{\int_0^\infty dt'\, C_{ij}(t')\,[a_i(t), a_j(t-t')\,\rho(t)] + \int_0^\infty dt'\, C_{ji}(-t')\,[\rho(t)\,a_j(t-t'), a_i(t)]\right\}. \tag{A1}$$

At this point we make use of the jump operators $A_{i,s}$ introduced in Eq. (29). They decompose a Majorana operator into a sum corresponding to individual transitions between eigenstates:

$$a_i = \sum_s (A_{i,s} + A_{i,s}^\dagger). \tag{A2}$$

We recall that $A_{i,s}$ are attached to transitions from odd-parity initial states to even-parity final states, and vice-versa $A_{i,s}^\dagger$ are attached to even-to-odd transitions. These operators have the nice property that

$$[H_A, A_{i,s}] = -\omega_s A_{i,s}. \tag{A3}$$

This enables one to write $a_i(t)$ as

$$a_i(t) = \sum_s [\exp(-i\omega_s t)A_{i,s} + \text{H.c.}]. \tag{A4}$$

The next step is to put back this expression for a_i into the master equation (A1). When doing so, we can make two considerations to reduce the number of terms that remain in the result. First, when there are two successive A operators multiplying ρ, they must correspond to opposite order of parity flips—so one A and one $A^\dagger$. Second, in the terms in which ρ is sandwiched between two A operators, the latter again should be of the opposite type if the initial ρ has no parity coherences, i.e., if $[\rho, P] = 0$ as discussed in the main text.

These selection rules considerably simplify the frequency mixing structure of the resulting master equation. Taking them into account, we obtain the identities

$$\begin{aligned}
&[a_i(t), a_j(t-t')\rho] \\
&\quad = \sum_{s,s'}[e^{-i(\omega_s-\omega_{s'})t}e^{i\omega_s t'}(A_{i,s'}^\dagger A_{j,s}\rho - A_{j,s}\rho A_{i,s'}^\dagger) + \text{H.c.}], \\
&[\rho a_j(t-t'), a_i(t)] \\
&\quad = \sum_{s,s'}[e^{i(\omega_s-\omega_{s'})t}\,e^{-i\omega_s t'}(\rho A_{j,s}A_{i,s'}^\dagger - A_{i,s'}^\dagger \rho A_{j,s}) + \text{H.c.}].
\end{aligned} \tag{A5}$$

Plugging these back into Eq. (A1), introducing the frequency differences $\delta_{ss'} = \omega_{s'} - \omega_s$, performing the integral over t',

and defining

$$\Gamma_{ij}(\omega) = \int_0^\infty dt\, \exp(i\omega t) C_{ij}(t), \tag{A6}$$

one finally obtains

$$\dot\rho = -\frac{1}{4}\sum_{i,j}\sum_{s,s'}[e^{i\delta_{ss't}}\,\Gamma_{ij}(\omega_s)(A^\dagger_{i,s'}A_{j,s}\rho - A_{j,s}\,\rho\,A^\dagger_{i,s'}) + e^{-i\delta_{ss't}}\,\Gamma_{ji}(-\omega_s)(A_{i,s'}A^\dagger_{j,s}\rho - A^\dagger_{j,s}\,\rho\,A_{i,s'}) + \text{H.c.}], \tag{A7}$$

of which we present in the main text the simplified version with $\Gamma_{ij}(\omega) = \delta_{ij}\Gamma(\omega)$. The more general decomposition of $\Gamma_{ij}(\omega)$ is $\Gamma_{ij}(\omega) = \frac{1}{2}\gamma_{ij}(\omega) + iS_{ij}(\omega)$ with

$$\gamma_{ij}(\omega) = \Gamma_{ij}(\omega) + \Gamma^*_{ji}(\omega), \tag{A8}$$

$$S_{ij}(\omega) = [\Gamma_{ij}(\omega) - \Gamma^*_{ji}(\omega)]/2i. \tag{A9}$$

Using the above definitions and simplifying the master equation (A1), we finally obtain the equation of the Bloch-Redfield form [Eq. (33)], quoted in Sec. IV.

APPENDIX B: BATH CORRELATION FUNCTIONS

To complete the Appendix, we provide a more explicit expression for the bath correlation function. Starting from Eq. (8), a standard equilibrium calculation yields

$$C_{ij}(t) = \sum_l \left[w_{il}w^*_{jl}\int_{-\infty}^\infty \nu_l(\epsilon)\, e^{-i\epsilon t} f(-\epsilon)\, d\epsilon + w^*_{il}w_{jl}\int_{-\infty}^\infty \nu_l(\epsilon)\, e^{i\epsilon t} f(\epsilon)\, d\epsilon \right], \tag{B1}$$

where $f(\epsilon)$ is the Fermi-Dirac distribution and $\nu_i(\epsilon)$ is the local density of states in reservoir i at the point contact position $\mathbf{r}_i$:

$$\nu_i(\epsilon) = \sum_k |\phi_k(\mathbf{r}_i)|^2\, \delta(\epsilon - \zeta_k). \tag{B2}$$

Here, the index k runs over a complete set of single-particle states of the reservoir, with energies ζ_k. For simplicity we will assume $\nu_i(\epsilon) \equiv \nu(\epsilon)$, the same for all four reservoirs. Then, we can decompose the correlation function as

$$C_{ij}(t) = z_{ij}\int_{-\infty}^\infty \nu(\epsilon)\, e^{-i\epsilon t} f(-\epsilon)\, d\epsilon + z^*_{ij}\int_{-\infty}^\infty \nu(\epsilon)\, e^{i\epsilon t} \tag{B3}$$

with

$$z_{ij} = \sum_l w_{il}w^*_{jl}, \tag{B4}$$

a complex number with the property $z_{ji} = z^*_{ij}$. By Fourier transform, we then obtain

$$\gamma_{ij}(\omega) = 2\pi[z_{ij}\nu(\omega) + z^*_{ij}\nu(-\omega)]\, f(-\omega). \tag{B5}$$

This function obeys the detailed balance condition

$$\gamma_{ji}(-\omega) = e^{-\beta\omega}\gamma_{ij}(\omega). \tag{B6}$$

Finally, using the fact that $C_{ij}(-t) = C^*_{ji}(t)$, we also find

$$S_{ij}(\omega) = -\frac{1}{2\pi}\,\text{p.v.}\int_{-\infty}^\infty \frac{\gamma_{ij}(\omega')}{\omega' - \omega}\, d\omega',$$

a Kramers-Krönig relation.

Disconnected reservoirs. In the simple case $w_{ij} = w\,\delta_{ij}$, often adopted in the main text, we have

$$z_{ij} = |w|^2\delta_{ij}. \tag{B7}$$

In this case, $C_{ij}(t) = \delta_{ij}C(t)$ with

$$C(t) = |w|^2\int_{-\infty}^\infty d\epsilon\, \nu(\epsilon)\left[\cos(\epsilon t) - i\tanh\left(\frac{1}{2}\beta\epsilon\right)\sin(\epsilon t)\right], \tag{B8}$$

and

$$\gamma(\omega) = 2\pi\,|w|^2\,\frac{\nu(\omega) + \nu(-\omega)}{1 + e^{-\beta\omega}}. \tag{B9}$$

Correlation functions for Sec. VC. The case of a zero-energy extended state case corresponds to the choice

$$w_{ij} = w_i\delta_{ij} + w_{12}\,\delta_{i1}\delta_{j2} + w_{21}\,\delta_{i2}\delta_{j1} \tag{B10}$$

for some complex numbers w_i, w_{12}, w_{21}. In this case, we have

$$z_{11} = |w_1|^2 + |w_{12}|^2, \tag{B11}$$

$$z_{12} = (w_1w^*_{21} + w_{12}w^*_2) = z^*_{21}, \tag{B12}$$

$$z_{22} = |w_2|^2 + |w_{21}|^2, \tag{B13}$$

$$z_{33} = |w_3|^2, \tag{B14}$$

$$z_{44} = |w_4|^2. \tag{B15}$$

The functions $\gamma_{ij}(\omega)$ can be obtained by replacement into Eq. (B5). It can be shown that $\gamma_{ij}(\omega)$ is positive if

$$z_{11}z_{22} \geqslant |z_{12}|^2, \tag{B16}$$

which is true for any choice of the parameters w_i, w_{12}, w_{21}. To simplify the mathematical treatment of this scenario, we then choose a symmetric situation in which $z_{11} = z_{22} = z_{33} = z_{44} = |w|^2$ and $z_{12} = \lambda|w|^2$. The positivity condition is satisfied if $|\lambda| \leqslant 1$. With this choice, one has

$$\gamma_{12}(\omega) = 2\pi\,|w|^2[\lambda\,\nu(\omega) + \lambda^*\nu(-\omega)]\, f(-\omega). \tag{B17}$$

If we further assume that $\nu(\omega) = \nu(-\omega)$, then this expression simplifies to

$$\gamma_{12}(\omega) = \lambda\gamma(\omega) \tag{B18}$$

with λ now real, and $-1 \leqslant \lambda \leqslant 1$. In this case, one finally gets

$$\gamma_{ij}(\omega) = \gamma(\omega)\,(\delta_{ij} + \lambda\,\delta_{i1}\delta_{j2} + \lambda\,\delta_{i2}\delta_{j1}). \tag{B19}$$

APPENDIX C: EXAMPLE OF A WIDE-BAND FERMIONIC BATH

In Sec. II, we introduced the bath correlation time τ_B and the dissipative timescale τ_D without specifying a microscopic model for the leads. In this Appendix, using a simple toy model for the fermionic reservoir, we provide explicit estimates of these two timescales, illustrating the separation

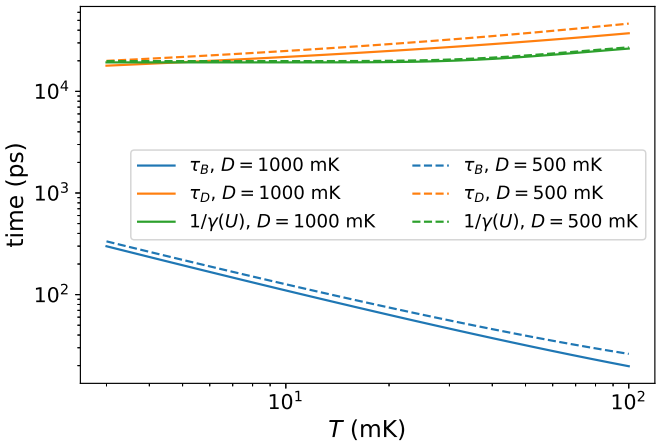


FIG. 3. Plots of the numerically calculated τ_B, τ_D, and $\gamma^{-1}(U)$, for the wide-band model of the bath. The two sets of results (in solid and dashed lines) are for two choices of $D = 1\,\mathrm{K}$, and $D = 0.5\,\mathrm{K}$, respectively. The value of $U = 100\,\mathrm{mK}$ for both curves. We observe a clear separation of scales $\tau_B \ll \tau_D$, and also the fact that $\gamma^{-1}(U) \sim \tau_D$ from the plots.

underlying the Born-Markov approximation used throughout the paper.

To obtain explicit estimates, we apply the formulas derived in the previous Appendix to the case in which the density of states is given by a broad Lorentzian,

$$\nu(\epsilon) = \frac{\nu(0)\,D^2}{\epsilon^2 + D^2}, \tag{C1}$$

where D is a soft bandwidth which provides a smooth realization of the wide-band limit. In particular, when

$$D \gg U,\ \epsilon,\ T, \tag{C2}$$

the spectral density varies weakly over the energy window relevant to the tetron dynamics. In the near-degenerate regime this allows, in particular, the replacement

$$\gamma(U \pm \epsilon_i) \simeq \gamma(U), \tag{C3}$$

discussed in Sec. V B.

We next consider the two timescales τ_B and τ_D introduced in Sec. II, Eq. (11) and Eq. (13), respectively. In the main text, we argued that $\tau_B^{-1} \approx k_B T$ whereas $\tau_D \approx \Gamma_0^{-1}$.

The correlation function $C(t)$ in Eq. (B8) depends on two time scales. The ultraviolet structure of $\nu(\epsilon)$ produces a short time scale of order D^{-1} and the Fermi factor introduces a parametrically longer thermal time scale of order $(\pi T)^{-1}$. The latter controls the long-time tail of the correlation function and can dominate the moment-defined correlation time τ_B in Eq. (11). Hence, $\tau_B = \mathcal{O}(1/\pi T)$, although the numerical prefactor is not universal because Eq. (11) involves $|C(t)|$ and retains some sensitivity to the ultraviolet line shape. Since $C(t)$ is proportional to Γ_0, its overall normalization cancels from Eq. (11) but not from (13). Hence, $\tau_D^{-1} \propto \Gamma_0 \propto |w|^2$, so that τ_D becomes parametrically long in the weak-coupling limit.

In Fig. 3, we plot the numerically calculated τ_B, τ_D, and $\gamma^{-1}(U)$ as functions of temperature for $U = 100\,\mathrm{mK}$ and $\Gamma_0 = 0.2\,\mathrm{mK}$. The two sets of curves, in solid and dashed lines, are for $D = 1.0\,\mathrm{K}$ and $D = 0.5\,\mathrm{K}$, respectively. In both cases, we see a clear separation of timescales $\tau_D \gg \tau_B$, which increases with temperature, as expected. Moreover, $\gamma^{-1}(U) \approx \Gamma_0 \approx \tau_D^{-1}$. The variation of $\gamma(\omega)$ around $\omega = U$ is within a few percent in an interval $U \pm 50\,\mathrm{mK}$.

APPENDIX D: DERIVATION OF THE MASTER EQUATION IN THE SECULAR REGIME

The derivation of the secular master equations uses the following consequences of the simple model adopted in the beginning of Sec. VI. First, $\epsilon_1 = \epsilon_2 = \epsilon$. Second, the odd-parity sector is doubly degenerate, while the energy splitting in the even-parity sector is 2ϵ. Third, the odd-to-even transition frequencies are $\omega_1 = \omega_2 = U - \epsilon$ and $\omega_3 = \omega_4 = U + \epsilon$. Fourth, the transition frequency differences $\delta_{ss'}$ split in two groups: The latter group includes the case with $s = s'$ as well as $(s, s') \in \{(1,2), (3,4), (2,1), (4,3)\}$. Fifth, the computational Majoranas a_i coincide with the eigenmodes $\tilde{a}_i$.

After all these considerations, and omitting all Lamb shift corrections proportional to $S(\omega)$, the Bloch-Redfield equation simplifies to

$$\begin{aligned}\dot{\rho} = &-\frac{1}{8}\gamma(U-\epsilon)\sum_i(\{L_{i,1}^\dagger L_{i,1}, \rho\} - 2L_{i,1}\,\rho\,L_{i,1}^\dagger)\\ &-\frac{1}{8}\gamma(\epsilon-U)\sum_i(\{L_{i,1}L_{i,1}^\dagger, \rho\} - 2L_{i,1}^\dagger\,\rho\,L_{i,1})\\ &-\frac{1}{8}\gamma(U+\epsilon)\sum_i(\{L_{i,2}^\dagger L_{i,2}, \rho\} - 2L_{i,2}\,\rho\,L_{i,2}^\dagger)\\ &-\frac{1}{8}\gamma(-U-\epsilon)\sum_i(\{L_{i,2}L_{i,2}^\dagger, \rho\} - 2L_{i,2}^\dagger\,\rho\,L_{i,2}).\end{aligned} \tag{D1}$$

Here, we have introduced the jump operators

$$L_{i,1} = A_{i,1} + A_{i,2} = \Pi_{--}\,a_i, \tag{D2}$$

$$L_{i,2} = A_{i,3} + A_{i,4} = \Pi_{++}\,a_i. \tag{D3}$$

Using Eqs. (29) and (30) it is possible to show that

$$\sum_i L_{i,1}^\dagger L_{i,1} = \sum_i L_{i,2}L_{i,2}^\dagger = \frac{1}{2}(1-P) \tag{D4a}$$

and

$$\sum_i L_{i,1}L_{i,1}^\dagger = 2\Pi_{--}, \tag{D4b}$$

$$\sum_i L_{i,2}L_{i,2}^\dagger = 2\Pi_{++}. \tag{D4c}$$

Performing the sums over i, we obtain the master equation in Eq. (71) of the main text.

APPENDIX E: REDUCTION OF THE UNIVERSAL LINDBLAD EQUATION

In this Appendix we show explicitly that the ULE dissipator in Eq. (84) reduces to the secular dissipator derived in Sec. VI for the symmetric geometry $A_{12} = A_{34} = \epsilon$. We assume disconnected and identical reservoirs and restrict the

dynamics to density matrices satisfying

$$[\rho, P] = 0. \tag{E1}$$

For compactness, we define

$$L_i \equiv L_{i,1} = \Pi_{--} a_i, \quad M_i \equiv L_{i,2} = \Pi_{++} a_i, \tag{E2}$$

and introduce

$$\begin{aligned} \gamma_- &= \gamma(U - \epsilon), \quad \bar{\gamma}_- = \gamma(\epsilon - U), \\ \gamma_+ &= \gamma(U + \epsilon), \quad \bar{\gamma}_+ = \gamma(-U - \epsilon). \end{aligned} \tag{E3}$$

The ULE jump operator in Eq. (86) is then

$$K_i = \sqrt{\gamma_-} L_i + \sqrt{\bar{\gamma}_-} L_i^\dagger + \sqrt{\gamma_+} M_i + \sqrt{\bar{\gamma}_+} M_i^\dagger. \tag{E4}$$

We first consider the anticommutator contribution to the dissipator. Since both Π_{--} and Π_{++} project onto states of even total parity, while each a_i changes the total parity,

$$\Pi_{\sigma\sigma} a_i \Pi_{\sigma'\sigma'} = 0, \quad \sigma, \sigma' = \pm 1. \tag{E5}$$

Together with $\Pi_{--}\Pi_{++} = 0$, this implies

$$L_i^2 = M_i^2 = L_i M_i = M_i L_i = 0, \tag{E6}$$

as well as the corresponding relations obtained by Hermitian conjugation. Moreover,

$$L_i^\dagger M_i = M_i^\dagger L_i = L_i M_i^\dagger = M_i L_i^\dagger = 0. \tag{E7}$$

All cross terms in $K_i^\dagger K_i$ therefore vanish identically, and one obtains

$$\begin{aligned} K_i^\dagger K_i = {} & \gamma_- L_i^\dagger L_i + \bar{\gamma}_- L_i L_i^\dagger \\ & + \gamma_+ M_i^\dagger M_i + \bar{\gamma}_+ M_i M_i^\dagger. \end{aligned} \tag{E8}$$

We next consider the recycling term. Expanding $K_i \rho K_i^\dagger$ gives the four diagonal contributions

$$\begin{aligned} K_i \rho K_i^\dagger\big|_{\text{diag}} = {} & \gamma_- L_i \rho L_i^\dagger + \bar{\gamma}_- L_i^\dagger \rho L_i \\ & + \gamma_+ M_i \rho M_i^\dagger + \bar{\gamma}_+ M_i^\dagger \rho M_i, \end{aligned} \tag{E9}$$

together with interference terms. For a density matrix obeying Eq. (E1), terms containing two operators with the same parity-changing orientation vanish. In particular,

$$\begin{aligned} & L_i \rho L_i = M_i \rho M_i = L_i \rho M_i = M_i \rho L_i = 0, \\ & L_i^\dagger \rho L_i^\dagger = M_i^\dagger \rho M_i^\dagger = L_i^\dagger \rho M_i^\dagger = M_i^\dagger \rho L_i^\dagger = 0. \end{aligned} \tag{E10}$$

The only remaining interference terms are therefore

$$L_i \rho M_i^\dagger, \quad M_i \rho L_i^\dagger, \quad L_i^\dagger \rho M_i, \quad M_i^\dagger \rho L_i. \tag{E11}$$

Unlike the terms in Eq. (E10), these do not vanish by total-parity selection alone. Their cancellation follows from the relative phases with which the two Majoranas of each canonical pair act on the eigenstates.

Indeed, the eigenstate projectors can be written as

$$\Pi_{\sigma\tau} = \tfrac{1}{4}(1 - \sigma P_{12})(1 - \tau P_{34}), \quad \sigma, \tau = \pm 1, \tag{E12}$$

and the Majorana operators within each pair satisfy

$$a_2 \Pi_{\sigma\tau} = -i\sigma\, a_1 \Pi_{\sigma\tau}, \quad a_4 \Pi_{\sigma\tau} = -i\tau\, a_3 \Pi_{\sigma\tau}. \tag{E13}$$

Equivalently,

$$\Pi_{\sigma\tau} a_2 = i\sigma\, \Pi_{\sigma\tau} a_1, \quad \Pi_{\sigma\tau} a_4 = i\tau\, \Pi_{\sigma\tau} a_3. \tag{E14}$$

Consider, for example, the interference term

$$\sum_i L_i \rho M_i^\dagger = \sum_i \Pi_{--} a_i \rho a_i \Pi_{++}. \tag{E15}$$

For the first Majorana pair, Eqs. (E13) and (E14) give

$$\Pi_{--} a_2 \rho a_2 \Pi_{++} = -\Pi_{--} a_1 \rho a_1 \Pi_{++}, \tag{E16}$$

and therefore

$$\sum_{i=1}^{2} \Pi_{--} a_i \rho a_i \Pi_{++} = 0. \tag{E17}$$

The same argument applied to the second Majorana pair gives

$$\sum_{i=3}^{4} \Pi_{--} a_i \rho a_i \Pi_{++} = 0. \tag{E18}$$

Hence,

$$\sum_i L_i \rho M_i^\dagger = 0. \tag{E19}$$

Hermitian conjugation gives

$$\sum_i M_i \rho L_i^\dagger = 0. \tag{E20}$$

The two remaining terms cancel in the same way,

$$\sum_i L_i^\dagger \rho M_i = \sum_i M_i^\dagger \rho L_i = 0. \tag{E21}$$

Combining Eqs. (E9)–(E21), the recycling term reduces to

$$\begin{aligned} \sum_i K_i \rho K_i^\dagger = {} & \gamma_- \sum_i L_i \rho L_i^\dagger + \bar{\gamma}_- \sum_i L_i^\dagger \rho L_i \\ & + \gamma_+ \sum_i M_i \rho M_i^\dagger + \bar{\gamma}_+ \sum_i M_i^\dagger \rho M_i. \end{aligned} \tag{E22}$$

Substitution of Eqs. (E8) and (E22) into Eq. (84) yields

$$\begin{aligned} \mathcal{D}_{\text{ULE}}[\rho] = {} & -\frac{\gamma_-}{8} \sum_i (\{L_i^\dagger L_i, \rho\} - 2 L_i \rho L_i^\dagger) \\ & - \frac{\bar{\gamma}_-}{8} \sum_i (\{L_i L_i^\dagger, \rho\} - 2 L_i^\dagger \rho L_i) \\ & - \frac{\gamma_+}{8} \sum_i (\{M_i^\dagger M_i, \rho\} - 2 M_i \rho M_i^\dagger) \\ & - \frac{\bar{\gamma}_+}{8} \sum_i (\{M_i M_i^\dagger, \rho\} - 2 M_i^\dagger \rho M_i). \end{aligned} \tag{E23}$$

Upon restoring the definitions in Eq. (E3), Eq. (E23) is identical to the dissipative part of the master equation in the secular regime.

[1] C. Nayak, S. H. Simon, A. Stern, M. Freedman, and S. Das Sarma, Non-Abelian anyons and topological quantum computation, Rev. Mod. Phys. **80**, 1083 (2008).

[2] S. Das Sarma, M. Freedman, and C. Nayak, Majorana zero modes and topological quantum computation, npj Quantum Inf. **1**, 15001 (2015).

[3] K. Flensberg, F. von Oppen, and A. Stern, Engineered platforms for topological superconductivity and Majorana zero modes, Nat. Rev. Mater. **6**, 944 (2021).

[4] M. Cheng, R. M. Lutchyn, and S. Das Sarma, Topological protection of Majorana qubits, Phys. Rev. B **85**, 165124 (2012).

[5] P. Bonderson and C. Nayak, Quasi-topological phases of matter and topological protection, Phys. Rev. B **87**, 195451 (2013).

[6] C. Knapp, T. Karzig, R. M. Lutchyn, and C. Nayak, Dephasing of Majorana-based qubits, Phys. Rev. B **97**, 125404 (2018).

[7] G. Goldstein and C. Chamon, Decay rates for topological memories encoded with Majorana fermions, Phys. Rev. B **84**, 205109 (2011).

[8] J. C. Budich, S. Walter, and B. Trauzettel, Failure of protection of Majorana based qubits against decoherence, Phys. Rev. B **85**, 121405 (2012).

[9] D. Rainis and D. Loss, Majorana qubit decoherence by quasiparticle poisoning, Phys. Rev. B **85**, 174533 (2012).

[10] T. Karzig, W. S. Cole, and D. I. Pikulin, Quasiparticle poisoning of Majorana qubits, Phys. Rev. Lett. **126**, 057702 (2021).

[11] A. Alase, M. C. Goffage, M. C. Cassidy, and S. N. Coppersmith, Decoherence of Majorana qubits by 1/f noise, arXiv:2506.22394.

[12] D. Aasen, M. Hell, R. V. Mishmash, A. Higginbotham, J. Danon, M. Leijnse, T. S. Jespersen, J. A. Folk, C. M. Marcus, K. Flensberg, and J. Alicea, Milestones toward Majorana-based quantum computing, Phys. Rev. X **6**, 031016 (2016).

[13] T. Karzig, C. Knapp, R. M. Lutchyn, P. Bonderson, M. B. Hastings, C. Nayak, J. Alicea, K. Flensberg, S. Plugge, Y. Oreg, C. M. Marcus, and M. H. Freedman, Scalable designs for quasiparticle-poisoning-protected topological quantum computation with Majorana zero modes, Phys. Rev. B **95**, 235305 (2017).

[14] D. Aasen, M. Aghaee, Z. Alam, M. Andrzejczuk, A. Antipov, M. Astafev, L. Avilovas, A. Barzegar, B. Bauer, J. Becker, J. M. Bello-Rivas, U. Bhaskar, A. Bocharov, S. Boddapati, D. Bohn, J. Bommer, P. Bonderson, J. Borovsky, L. Bourdet, S. Boutin, *et al.*, Blueprint for fault-tolerant quantum computation with topological qubit arrays, Phys. Rev. Res. **7**, 041002 (2025).

[15] L. Fu, Electron teleportation via Majorana bound states in a mesoscopic superconductor, Phys. Rev. Lett. **104**, 056402 (2010).

[16] S. Vijay and L. Fu, Teleportation-based quantum information processing with Majorana zero modes, Phys. Rev. B **94**, 235446 (2016).

[17] S. Plugge, A. Rasmussen, R. Egger, and K. Flensberg, Majorana box qubits, New J. Phys. **19**, 012001 (2017).

[18] C. Schrade and L. Fu, Majorana superconducting qubit, Phys. Rev. Lett. **121**, 267002 (2018).

[19] M. Aghaee, A. Akkala, Z. Alam, R. Ali, A. Alcaraz Ramirez, M. Andrzejczuk, A. E. Antipov, P. Aseev, M. Astafev, B. Bauer, J. Becker, S. Boddapati, F. Boekhout, J. Bommer, T. Bosma, L. Bourdet, S. Boutin, P. Caroff, L. Casparis, M. Cassidy, *et al.*, (Microsoft Quantum), InAs-Al hybrid devices passing the topological gap protocol, Phys. Rev. B **107**, 245423 (2023).

[20] M. Aghaee, A. Alcaraz Ramirez, Z. Alam, R. Ali, M. Andrzejczuk, A. Antipov, M. Astafev, A. Barzegar, B. Bauer, J. Becker, U. K. Bhaskar, A. Bocharov, S. Boddapati, D. Bohn, J. Bommer, L. Bourdet, A. Bousquet, S. Boutin, L. Casparis, B. J. Chapman, *et al.*, Interferometric single-shot parity measurement in InAs–Al hybrid devices, Nature (London) **638**, 651 (2025).

[21] M. Aghaee, Z. Alam, M. Andrzejczuk, A. Antipov, T. Asimakidis, M. Astafev, L. Avilovas, A. Azizimanesh, A. Barzegar, B. Bauer, J. Becker, U. K. Bhaskar, A. G. Boa, S. Boddapati, N. Bohac, J. Bommer, J. Borovsky, L. Bourdet, S. Boutin, S. Chakravarthi, *et al.*, 20 second parity lifetime in an InAs–Pb tetron device, arXiv:2606.03884.

[22] S. Das Sarma, In search of Majorana, Nat. Phys. **19**, 165 (2023).

[23] H. F. Legg, On the robustness of topological gap detection via transport, Nature (London) **654**, E22 (2026).

[24] Microsoft Quantum, Reply to: On the robustness of topological gap detection via transport, Nature (London) **654**, E27 (2026).

[25] M. Aghaee, Z. Alam, R. Andersen, M. Andrzejczuk, A. Antipov, M. Astafev, L. Avilovas, A. Azizimanesh, E. Banek, B. Bauer, J. Becker, U. K. Bhaskar, A. G. Boa, S. Boddapati, N. Bohac, J. D. S. Bommer, J. Borovsky, L. Bourdet, S. Boutin, L. Casparis, *et al.*, Distinct lifetimes for X and Z loop measurements in a Majorana tetron device, arXiv:2507.08795.

[26] N. van Loo, F. Zatelli, G. O. Steffensen, B. Roovers, G. Wang, T. Van Caekenberghe, A. Bordin, D. van Driel, Y. Zhang, W. D. Huisman, G. Badawy, E. P. A. M. Bakkers, G. P. Mazur, R. Aguado, and L. P. Kouwenhoven, Single-shot parity readout of a minimal Kitaev chain, Nature (London) **650**, 334 (2026).

[27] F. Zatelli, B. Roovers, N. van Loo, A. Lombardi, J. D. T. Luna, S. Miles, V. P. M. Sietses, F. J. B. Evertsz', P. C. Fariña, A. Bordin, G. Badawy, E. P. A. M. Bakkers, M. Wimmer, and L. P. Kouwenhoven, Majorana parity qubit in coupled minimal Kitaev chains, arXiv:2607.09511.

[28] J. D. Sau and S. Das Sarma, Realizing a robust practical Majorana chain in a quantum-dot-superconductor linear array, Nat. Commun. **3**, 964 (2012).

[29] T. Dvir, G. Wang, N. van Loo, C.-X. Liu, G. P. Mazur, A. Bordin, S. L. D. ten Haaf, J.-Y. Wang, D. van Driel, F. Zatelli, X. Li, F. K. Malinowski, S. Gazibegovic, G. Badawy, E. P. A. M. Bakkers, M. Wimmer, and L. P. Kouwenhoven, Realization of a minimal Kitaev chain in coupled quantum dots, Nature (London) **614**, 445 (2023).

[30] S. L. D. ten Haaf, Y. Zhang, Q. Wang, A. Bordin, C.-X. Liu, I. Kulesh, V. P. M. Sietses, C. G. Prosko, D. Xiao, C. Thomas, M. J. Manfra, M. Wimmer, and S. Goswami, Observation of edge and bulk states in a three-site Kitaev chain, Nature (London) **641**, 890 (2025).

[31] H. Pan, S. Das Sarma, and C.-X. Liu, Rabi and Ramsey oscillations of a Majorana qubit in a quantum dot-superconductor array, Phys. Rev. B **111**, 075416 (2025).

[32] M. Nitsch, L. Maffi, V. V. Baran, R. Seoane Souto, J. Paaske, M. Leijnse, and M. Burrello, Poor man's Majorana tetron, PRX Quantum **6**, 030365 (2025).

[33] H.-P. Breuer and F. Petruccione, *The Theory of Open Quantum Systems* (Oxford University Press Oxford, 2002).

[34] E. Mozgunov and D. Lidar, Completely positive master equation for arbitrary driving and small level spacing, Quantum **4**, 227 (2020).

[35] F. Nathan and M. S. Rudner, Universal Lindblad equation for open quantum systems, Phys. Rev. B **102**, 115109 (2020).

[36] Noise in the parameters of the Hamiltonian (2) could be, for instance, due to charge noise and could be a significant source of dephasing in tetron devices [6]. We note that charge noise can also affect the parameter U, however since U couples to total parity P, this would be a common noise mode for the two qubit states. Fluctuations in U can affect parity-changing transitions and their rates, but we do not consider this effect in this work.

[37] R. V. Mishmash, B. Bauer, F. von Oppen, and J. Alicea, Dephasing and leakage dynamics of noisy Majorana-based qubits: Topological versus Andreev, Phys. Rev. B **101**, 075404 (2020).

[38] S. Bhattacharyya, M. Grilli, and B. van Heck, Decoherence of Majorana zero modes mediated by gapless fermions, Phys. Rev. B **113**, 035422 (2026).

[39] M. I. K. Munk, J. Schulenborg, R. Egger, and K. Flensberg, Parity-to-charge conversion in Majorana qubit readout, Phys. Rev. Res. **2**, 033254 (2020).

[40] S. Boutin, T. Karzig, T. E. Dandachi, R. V. Mishmash, J. Gukelberger, R. M. Lutchyn, and B. Bauer, Predictive simulations of the dynamical response of mesoscopic devices, arXiv:2502.12960.

[41] A. Vuik, B. Nijholt, A. R. Akhmerov, and M. Wimmer, Reproducing topological properties with quasi-Majorana states, SciPost Phys. **7**, 061 (2019).

[42] F. L. Pedrocchi and D. P. DiVincenzo, Majorana braiding with thermal noise, Phys. Rev. Lett. **115**, 120402 (2015).

[43] H.-L. Lai and W.-M. Zhang, Decoherence dynamics of Majorana qubits under braiding operations, Phys. Rev. B **101**, 195428 (2020).

[44] D. Sahu and S. Gangadharaiah, Noisy braiding of Majorana modes: A comparison of nanowire trijunction and quantum-dot-assisted architectures, arXiv:2608.09416.